Widely tunable soliton frequency shifting of few-cycle laser pulses

N. Ishii,[1] C. Y. Teisset,[1] S. Köhler,[1] E. E. Serebryannikov,[2] T. Fuji,[1] T. Metzger,[1] F. Krausz,[1,3] A. Baltuška,[1,*] and A. M. Zheltikov[2,†]

[1]*Max-Planck-Institut für Quantenoptik, Hans-Kopfermann-Strasse 1, D-85748 Garching, Germany*

[2]*Physics Department, International Laser Center, M. V. Lomonosov Moscow State University, Vorob'evy gory, Moscow 119992, Russia*

[3]*Department für Physik, Ludwig-Maximilians-Universität Munich, D-85748 Garching, Germany*

(Received 7 October 2005; published 18 September 2006)

Photonic-crystal fibers are employed to demonstrate widely tunable frequency down-conversion of unamplified 6-fs Ti:sapphire laser pulses through the soliton self-frequency shift induced by the Raman effect. Wavelength shifts as large as 500 nm are achieved for input few-cycle pulses with broadband spectra centered at approximately 820 nm. The central wavelength of the redshifted output of a photonic-crystal fiber is smoothly tuned from the low-frequency edge in the spectrum of the 6-fs Ti:sapphire laser pulse up to 1.35 μm by varying the input energy in the fundamental mode of the fiber.

DOI: 10.1103/PhysRevE.74.036617 PACS number(s): 42.65.Wi

I. INTRODUCTION

Recent revolutionary breakthroughs in laser science have resulted in the development of a new generation of laser sources capable of routinely delivering radiation pulses as short as a few cycles of the light field [1,2]. With the advent of such unique light sources, the key issue on the agenda is the development of equally efficient and convenient frequency converters that would allow the wavelength shifting of few-cycle laser pulses. Such frequency shifters would make few-cycle pulses an indispensable tool for the investigation of ultrafast processes in physics, chemistry, and biology, promoting applications of ultrashort pulse sources for metrological, spectroscopic, and biomedical applications [3–5]. Few-cycle laser pulses directly from a laser oscillator are typically characterized by a low field intensity distributed over a broad spectral range. Such field wave forms are challenging objects for nonlinear-optical frequency converters because of the difficulties related to the low field intensity and the large bandwidth of unamplified few-cycle laser pulses.

The most successful and practical strategies of frequency conversion of few-cycle pulses are currently based on ultrafast-optics modifications of optical parametric amplification (OPA) [6–8] and optical parametric chirped-pulse amplification (OPCPA) [9–14] schemes. These efficient and elegant approaches involve frequency conversion and simultaneous amplification of low-spectral-intensity ultrabroadband field wave forms (few-cycle pulses or white-light emission) in the field of a more powerful pump field. Here we show that, along with these parametric amplification options, efficient spectral transformation of few-cycle laser pulses can be based on self-frequency conversion. Unlike parametric amplification schemes, self-frequency conversion does not require application of any additional powerful pump field. It will be demonstrated in this work, both experimentally and theoretically, that efficient self-frequency conversion strategies can be realized through the soliton evolution of few-cycle field wave forms in optical fibers of a new type—photonic-crystal fibers (PCFs) [15,16]. These fibers are presently giving a new momentum to the nonlinear optics of ultrashort pulses, providing large interaction lengths [17], strong confinement of electromagnetic field in a small fiber core [18], and offering a unique flexibility in dispersion engineering [19]. Enhanced nonlinear-optical processes in PCFs make these fibers ideal sources of supercontinuum emission [20,21], giving an excess to the carrier–envelope phase [22], allowing the generation of stabilized frequency combs for optical metrology and femtosecond clockwork [23], permitting creation of novel optical coherence tomographs [24], improving the performance of nonlinear spectrographs [25] and microscopes [26], and expanding the applicability range of femtosecond laser sources to photochemistry and photobiology [27]. Due to their remarkable dispersion properties, unattainable with standard optical fibers, PCFs support new soliton regimes and allow observation of novel solitonic phenomena [28], suggesting attractive solutions for the soliton transmission and transformation of ultrashort laser pulses.

Optical solitons propagating in the media with noninstantaneous nonlinear response experience reshaping and continuous frequency down-shifting due to the Raman effect–phenomenon, called soliton self-frequency shift (SSFS) [29–31]. Photonic-crystal fibers substantially enhance this nonlinear-optical process due to a strong field confinement in a small-size fiber core and the possibility to tailor dispersions of guided modes by varying the fiber structure. Liu *et al.* [32] have shown that 200-fs input pulses of 1.3-μm laser radiation can generate sub-100-fs soliton pulses with a central wavelength tunable down to 1.65 μm through the SSFS in a tapered PCF. Photonic-crystal fibers with the wavelength of zero group-velocity dispersion (GVD) shifted to shorter wavelengths have been used for the soliton frequency down-shifting of 800–1050-nm laser pulses [33,34]. Abedin and Kubota [35] have employed a PCF to demonstrate a 120-nm SSFS for 10-GHz-repetition-rate picosecond pulses. In our recent work [36], PCFs with a special dispersion profile have been shown to provide an efficient spectral transformation of chirped sub-6-fs Ti:sapphire laser pulses through

*E-mail address: andrius.baltuska@mpq.mpg.de

†E-mail address: zheltikov@phys.msu.ru

SSFS, leading to the generation of a well-resolved solitonic spectral component centered at 1.06 μm. Redshifted soliton signals formed by 6-fs laser pulses in PCFs have been demonstrated to allow a synchronized seeding of a picosecond Nd: YAG (yttrium aluminum garnet) pump laser, permitting a considerable simplification of a few-cycle OPCPA scheme [37].

In this work, we extend the SSFS-based strategy of tunable frequency conversion to few-cycle laser pulses. Earlier studies [38] have revealed interesting features of SSFS of pulses with an initial pulse width of 12 fs. We will show here that the use of 6-fs laser pulses allows a substantial enhancement of SSFS, leading to higher frequency shifting rates of solitons in PCFs. Experiments and numerical simulations presented below in this paper demonstrate a widely tunable frequency down-conversion of unamplified 6-fs Ti:sapphire laser pulses through the SSFS in PCFs. Wavelength shifts as large as 500 nm are achieved for input pulses with broadband spectra centered at approximately 820 nm, providing radiation with a central wavelength smoothly tunable from the central wavelength of the input pulse to 1.32 μm and energies ranging from a few up to tens of picojoules.

II. MODELING THE SOLITON EVOLUTION OF FEW-CYCLE PULSES IN PHOTONIC-CRYSTAL FIBERS

With many of the key tendencies in the evolution of ultrashort pulses in PCFs analyzed in the extensive literature, we focus here on the possibility of using the SSFS phenomenon for widely tunable frequency shifting of few-cycle laser pulses. Our theoretical analysis is based on the numerical solution of the generalized nonlinear Schrödinger equation (GNSE) [31]

$$\frac{\partial A}{\partial z} = i\sum_{k=2}^{6} \frac{(i)^k}{k!}\beta^{(k)}\frac{\partial^k A}{\partial \tau^k} + i\gamma\left(1+\frac{i}{\omega_0}\frac{\partial}{\partial \tau}\right)\left(A(z,\tau)\int_{-\infty}^{\infty} R(\eta) \times |A(z,\tau-\eta)|^2 d\eta\right), \quad (1)$$

where A is the field amplitude, $\beta^{(k)}=\partial^k\beta/\partial\omega^k$ are the coefficients in the Taylor-series expansion of the propagation constant β, ω_0 is the carrier frequency, τ is the retarded time, $\gamma=(n_2\omega_0)/(cS_{eff})$ is the nonlinear coefficient, n_2 is the nonlinear refractive index of the PCF material,

$$S_{eff} = \left[\int_{-\infty}^{\infty}\int_{-\infty}^{\infty}|F(x,y)|^2 dx\, dy\right]^2 \Big/ \int_{-\infty}^{\infty}\int_{-\infty}^{\infty}|F(x,y)|^4 dx\, dy$$

is the effective mode area [$F(x,y)$ is the transverse field profile in the PCF mode], and $R(t)$ is the retarded nonlinear response function. For fused silica, we take $n_2 \approx 3.2 \times 10^{-16}$ cm^2/W, and the $R(t)$ function is represented in a standard form [39]:

$$R(t) = (1-f_R)\delta(t) + f_R\Theta(t)\frac{\tau_1^2+\tau_2^2}{\tau_1\tau_2^2}e^{-t/\tau_2}\sin\left(\frac{t}{\tau_1}\right), \quad (2)$$

where $f_R=0.18$ is the fractional contribution of the Raman response; $\delta(t)$ and $\Theta(t)$ are the delta and the Heaviside step functions, respectively; $\tau_1=12.5$ fs and $\tau_2=32$ fs are the characteristic times of the Raman response of fused silica.

Equations (1) and (2) will be applied here to compute the evolution of ultrashort pulses in three types of PCFs. PCFs of the first and second types, shown in insets 1 and 2 to Fig. 1, respectively, represent an extensively employed class of microstructure fibers characterized by a high-air-filling fraction of the cladding, which typically consists of only a few cycles of air holes. The high content of air in the cladding of such PCFs strongly confines the light field to the fiber core, enhancing nonlinear-optical interactions. In PCFs of these types used in the experiments presented below in this paper, a fused silica core with a diameter of 1.6 μm (for first-type PCFs, see inset 1 in Fig. 1) or 2.6 μm (for second-type PCFs, inset 2 in Fig. 1) was surrounded with two cycles of air holes.

To find parameters $\beta^{(k)}$ and the effective mode area S_{eff} for these fibers, we numerically solve the Maxwell equations for the transverse components of the electric field in the cross section of a PCF using a modification of the method of polynomial expansion in localized functions, developed by Monro *et al.* [40]. The polynomial approximation of the frequency dependence of the propagation constant β for the fundamental mode of the 1.6-μm-core-diameter PCF computed with the use of this numerical procedure with an accuracy better than 0.1% within the range of wavelengths from 580 to 1220 nm yields the following $\beta^{(k)}$ coefficients for the central wavelength of 800 nm: $\beta^{(2)} \approx -0.0293$ ps^2/m, $\beta^{(3)} \approx 9.316\times10^{-5}$ ps^3/m, $\beta^{(4)} \approx -9.666\times10^{-8}$ ps^4/m, $\beta^{(5)} \approx 1.63\times10^{-10}$ ps^5/m, $\beta^{(6)} \approx -3.07\times10^{-13}$ ps^6/m. Curve 1 in Fig. 1 displays the GVD $D=-2\pi c\lambda^{-2}\beta^{(2)}$, where λ is the radiation wavelength, for the fundamental mode of such PCFs as a function of the wavelength. The GVD vanishes in this case at $\lambda_z \approx 690$ nm. For 800-nm radiation, the effective mode area S_{eff} was equal to 2.0 μm^2 for the first-type PCF and 4.5 μm^2 for the second-type PCF. The nonlinear coefficients for these fibers at 800 nm are estimated as 120 and 50 (W km)$^{-1}$, respectively.

Fibers of the third type are commercial NL-PM-750 PCFs from crystal fibre [41]. The core diameter for these PCFs was equal to 1.8 μm. Parameters $\beta^{(k)}$ for these PCFs were defined as polynomial expansion coefficients for the dispersion profile of the fundamental mode of these fibers provided by the manufacturer [41]. The group-velocity dispersion for PCFs of this type is presented by curve 2 in Fig. 1. In this case, the GVD vanishes at $\lambda_z \approx 750$ nm. For 800-nm radiation, the effective mode area for this type of PCF is 2.2 μm^2, corresponding to a nonlinear coefficient of about 110 (W km)$^{-1}$.

III. TUNING THE SOLITON SELF-FREQUENCY SHIFT OF FEW-CYCLE PULSES

In Figs. 2(a)–2(d), we illustrate tunable frequency shifting of few-cycle laser pulses through SSFS in PCFs by presenting the results of simulations performed for an idealistic input pulse with an initial pulse width of 6 fs and a Gaussian pulse shape. For a PCF with a dispersion profile as shown by curve 1 in Fig. 1, almost the entire spectrum of the input

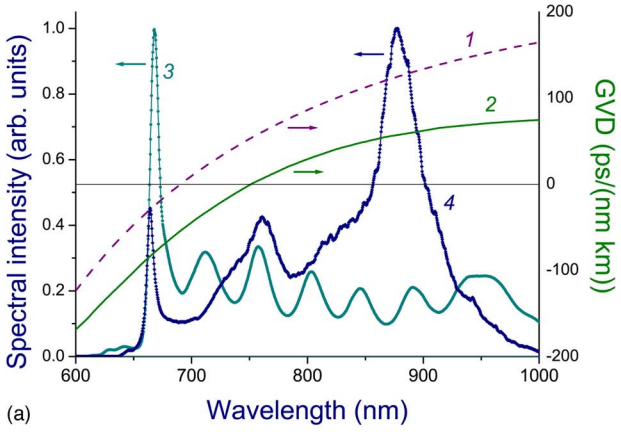

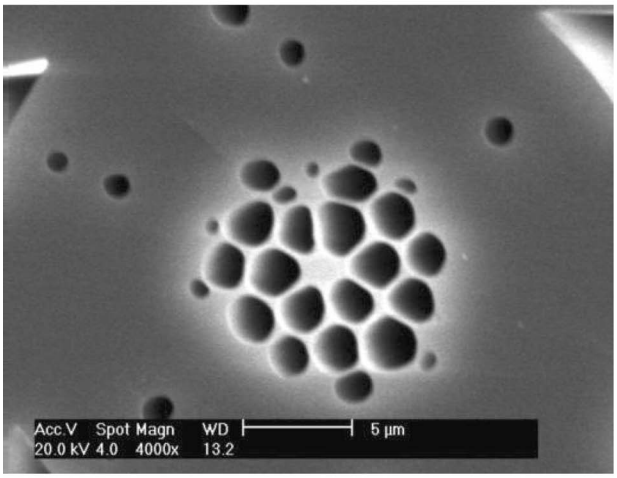

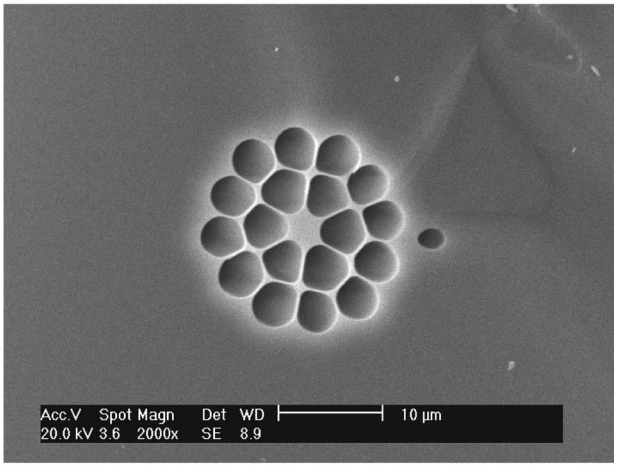

FIG. 1. (Color online) The group-velocity dispersion (GVD) as a function of the wavelength for the fundamental mode of (1) a fused silica photonic-crystal fiber with a high-air-filling-fraction cladding consisting of two cycles of air holes surrounding a core with a diameter of 1.6 μm (shown in inset 1) and (2) NL-PM-750 PCF from crystal fibre. Also shown are the intensity spectra of few-cycle input laser pulses provided by a Ti:sapphire oscillator with different sets of chirped mirrors (3, 4). The insets present scanning electron microscopy images of fused silica PCFs with a core diameter of 1.6 μm (1) and 2.6 μm (2).

pulse falls within the range of anomalous dispersion, and the pulse tends to form solitons, observed as well-resolved prominent spikes in the time domain [Figs. 2(a) and 2(b)]. In the frequency domain, the Raman effect leads to a continuous frequency downshifting of the soliton [Figs. 2(c) and 2(d)]. The rate of this frequency shift $d\nu/dz$, where ν is the carrier frequency and z is the propagation coordinate, rapidly grows with a decrease in the pulse duration τ_0. With a linear approximation of the Raman gain as a function of the frequency, the integration of the nonlinear Schrödinger equation, as shown by Gordon [42], yields $d\nu/dz \propto \tau_0^{-4}$. Although high-order dispersion and deviations of the Raman gain curve from the linear function generally make the relation between $d\nu/dz$ and τ in soliton dynamics much more complicated [43], the soliton pulse width remains one of the key parameters controlling the soliton frequency shift for a given Raman gain profile. In the case considered here, the short duration of 6-fs input pulses provides a high rate of soliton frequency shifting at the initial stage of pulse propagation through the PCF. As the spectrum of the soliton is shifted toward the spectral range with larger values of GVD, the pulse width increases, which slows down the frequency shift.

Input pulses with higher energies can be coupled into shorter solitons, leading to higher SSFS rates. Indeed, as can be seen from the comparison of the results of simulations performed for input pulses with the same initial pulse width (6 fs), but different energies, the SSFS rate in the case of higher energy pulses can substantially exceed the frequency-shift rate of solitons produced by lower energy pulses. A pulse with an input energy of 0.15 nJ, as can be seen from Fig. 2(c), is coupled into a soliton, which undergoes a permanent redshift as it propagates through the fiber. At z =30 cm, the spectrum of this soliton peaks at 1.06 μm. A similar input pulse that has an initial energy of 0.5 nJ forms a soliton that exhibits a much faster frequency downshift. The central wavelength of this soliton reaches 1.12 μm already at z=5 cm.

To provide illustrative physical insights into the observed behavior of redshifted solitons in PCFs as a function of the input pulse energy, we plot in Fig. 3 the snapshots of temporal envelopes of the solitonic part of the field corresponding to the input energies of 0.15 nJ (curve 1) and 0.5 nJ (curve 2). We take these snapshots of solitons, representing closeup views of intensity envelope sections labeled with boxes in Figs. 2(a) and 2(b), for two different values of the propagation coordinate, z=30 cm in the case of a 0.15-nJ input pulse and z=3 cm for the 0.5-nJ input energy. With the spectra of redshifted solitons centered around 1.06 μm in both cases [see Figs. 2(c) and 2(d)], these values of the propagation coordinate allow a fair comparison of SSFS dynamics in terms of the dependence of the frequency-shift rate on the soliton pulse width. As is seen from Fig. 3, the SSFS rate correlates well with the soliton pulse width. While the soliton produced by a pulse with an initial energy of 0.15 nJ has a pulse width of about 50 fs (curve 1 in Fig. 3), the pulse width of the soliton emerging from the 0.5-nJ laser pulse is about 20 fs. In qualitative agreement with predictions of Gordon [42], this shorter soliton in Figs. 2(b) and 2(d) displays a faster downshifting as compared with the longer soliton in Figs. 2(a) and 2(c). In the following section, this dependence

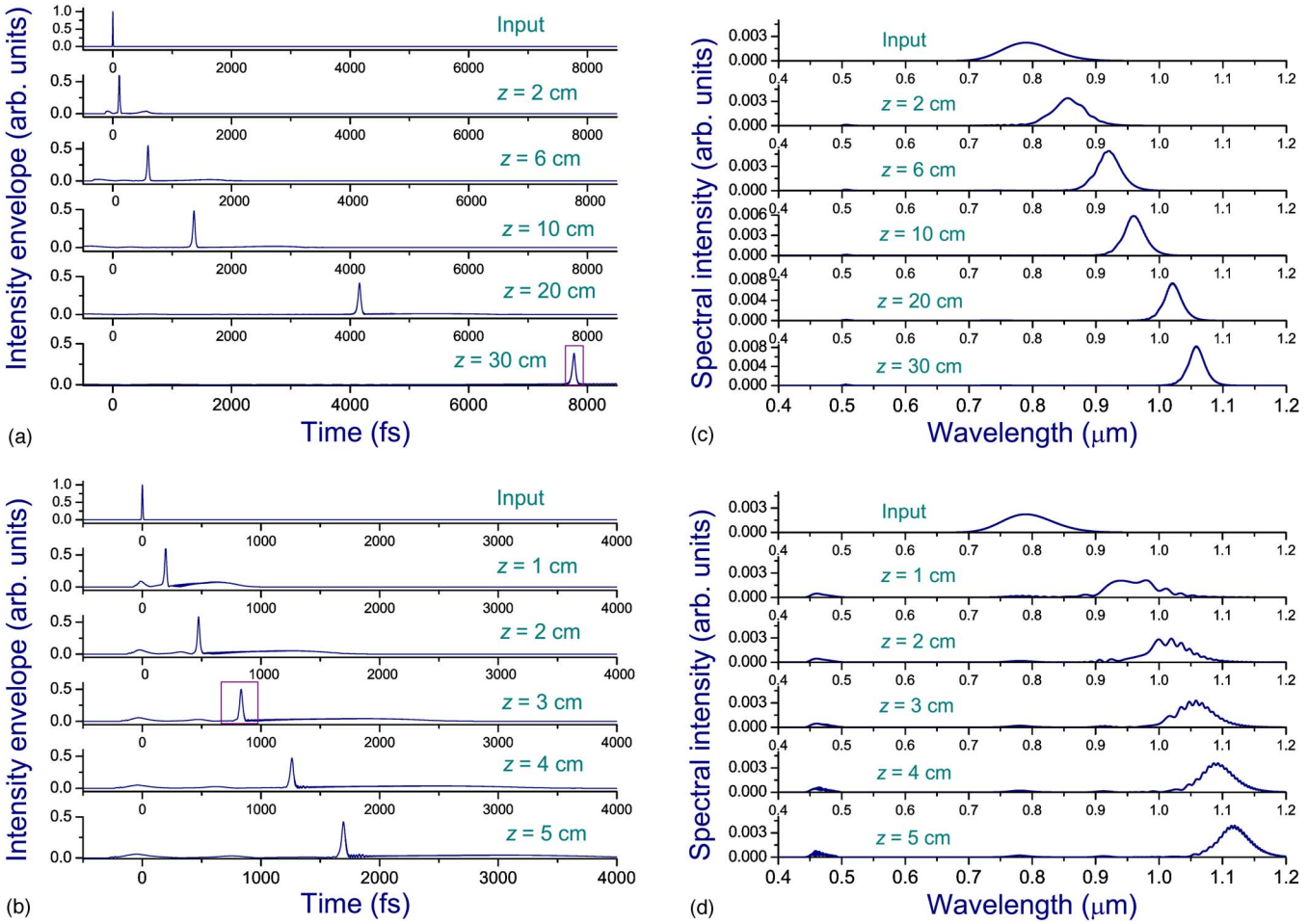

FIG. 2. (Color online) Temporal (a) and (b) and spectral (c) and (d) evolution of laser pulses with an initial energy of (a) and (c) 0.15 nJ and (b) and (d) 0.5 nJ and an initial pulse width of 6 fs in a PCF with a dispersion profile shown by curve 1 in Fig. 1. The input pulses are assumed to be transform-limited.

of the SSFS rate on the energy of the pulse launched into the fiber will be used for the experimental demonstration of a widely tunable soliton frequency shift of 6-fs pulses produced by a Ti:sapphire oscillator.

The GVD of PCFs changes very substantially across the broad spectrum of few-femtosecond laser pulses used in our experiments, ranging from $-(50-100)$ ps/(nm km) on the short-wavelength wing of the spectrum to $80-170$ ps/(nm km) on its long-wavelength tail (Fig. 1). This indicates the importance of high-order dispersion terms in Eq. (1), involving $\beta^{(k)}$ parameters with $k>2$. In this regime, it generally becomes difficult to use the results of the analysis of ideal solitons, i.e., solitons governed by the nonlinear Schrödinger equation (NLSE), even for a qualitative interpretation of numerical simulations and experimental data. With the GVD changing so drastically across the spectrum of the laser pulse, the basic soliton parameters, including the soliton number and the soliton amplitude in the canonical form of the NLSE, are no longer well defined. For a PCF with a core diameter of 2.6 μm, for example, the soliton number $N=(\gamma P_0 \tau_0^2/|\beta_2|)^{1/2}$, where P_0 is the peak power and τ_0 is the soliton pulse width, changes from 16.3 at 820 nm (in the region close to the zero-GVD wavelength) to 1.9 at 950 nm. These changes in soliton parameters across the spectrum of the laser pulse imply that the well-established methods of soliton analysis cannot be employed. Because of substantial GVD variations across the pulse spectrum, it becomes difficult, in particular, to pose the corresponding scattering problem, as a specific GVD value is needed to specify the normalization of the scattering potential.

In this regime, the method of analysis based on the GNSE [Eq. (1)] seems to be the most adequate approach. Results of simulations presented in Figs. 2(c) and 2(d) suggest that the SSFS in PCFs can shift the central wavelength of one of the intense components in the field spectrum by more than 300 nm relative to the central wavelength of the input field [Fig. 2(d)]. This prediction is consistent with the results of earlier experimental studies on SSFS in PCFs [32], as well as with the experimental data presented below in this paper. A special care should be taken in this regime in applying the SVEA and, more generally, in choosing approximations concerning the variation rate of the field envelope. It should be noted in this context that GNSE-type equations [e.g., Eq. (1) of this paper], as shown by Brabec and Krausz [43], do not require the standard SVEA assumption that the field cycle should be much smaller than the pulse width. As demonstrated in [43], this type of equation can be rather classified

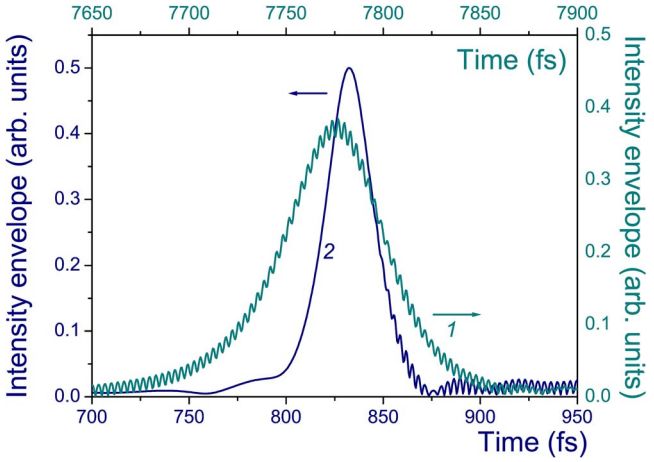

FIG. 3. (Color online) Temporal envelopes of redshifted solitons (close-up of the peaks labeled with boxes in 2(a) and 2(b) generated by laser pulses with an initial pulse width of 6 fs and an initial energy of (1) 0.15 nJ and (2) 0.5 nJ in a PCF at $z=30$ cm (1) and 3 cm (2).

as a slowly evolving wave approximation and can accurately describe the nonlinear evolution of light pulses down to the single-cycle regime.

IV. EXPERIMENTAL RESULTS AND DISCUSSION

In experiments, we used a broadband chirped-mirror Ti:sapphire oscillator [44], generating 6-fs pulses with an energy up to 4 nJ at a repetition rate of 70 MHz. The laser output was divided into two channels of roughly equal energies with a beamsplitter. One of the resulting beams was reserved for pumping a Nd:YAG regenerative amplifier [37], while the second beam was sent into the PCF, providing, with allowance for fiber-coupling losses, initial pulse energies in the nano- to sub-nano-joule range.

Curves 3 and 4 in Fig. 1 display the output intensity spectra of the Ti:sapphire oscillator with two different sets of chirped mirrors. The pulse width in both cases was about 6 fs (curve 1 in Fig. 4). In Fig. 5, we illustrate the spectral evolution of laser pulses in a fiber with a dispersion profile of

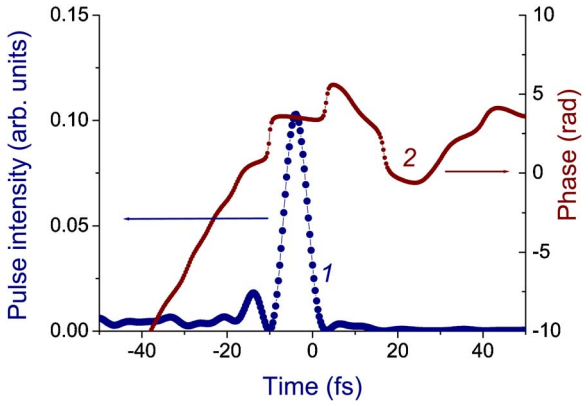

FIG. 4. (Color online) Temporal envelope (1) and chirp (2) of the Ti:sapphire oscillator output reconstructed from SPIDER data.

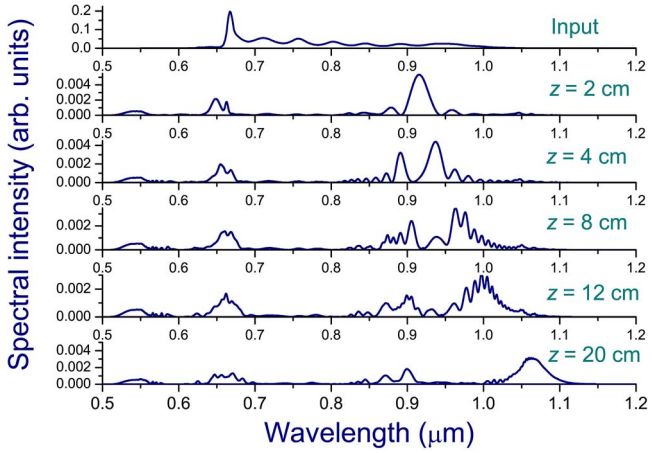

FIG. 5. (Color online) Spectral evolution of a laser pulse with an initial energy of 0.33 nJ and an input temporal envelope and chirp shown in Fig. 4 propagating through the PCF with the dispersion profile as presented by curve 2 in Fig. 1.

the NL-PM-750 PCF (curve 2 in Fig. 1), simulated for the realistic input temporal envelope and initial chirp of laser pulses as defined by SPIDER measurements for the output of the above-described Ti:sapphire oscillator (Fig. 4). In the case of few-cycle laser pulses with a realistic initial chirp (shown by curve 2 in Fig. 4), a significant amount of input pulse energy can propagate in a fiber in the form of nonsolitonic radiation, contributing to the background observed between the prominent spectral peaks, related to four-wave mixing (FWM) and soliton phenomena [cf. Figs. 2(d) and 5].

The initial stage of nonlinear-optical transformation of few-cycle pulses in a PCF involves self-phase modulation, which can be viewed as four-wave mixing of different frequency components belonging to the broad spectrum of radiation propagating through the fiber. Frequency components lying near the zero-GVD wavelength of the PCF then serve, as shown in the classical texts on nonlinear fiber optics [31], as a pump for phase-matched FWM. Such phase-matched FWM processes, which involve both frequency-degenerate and frequency-nondegenerate pump photons, deplete the spectrum of radiation around the zero-GVD wavelength and transfer the radiation energy to the region of anomalous dispersion (spectral components around 920 nm for $z=2$ cm in Fig. 5). A part of this frequency-downconverted radiation then couples into a soliton, which undergoes continuous frequency downshifting due to the Raman effect (Fig. 5). In the time domain, the redshifted solitonic part of the radiation field becomes delayed with respect to the rest of this field because of the anomalous GVD of the fiber. As a result of these processes, the redshifted soliton becomes more and more isolated from the rest of the light field in both time and frequency domain, which reduces, in particular, the interference between the solitonic and nonsolitonic part of radiation, seen in Figs. 2(d) and 5.

High-order fiber dispersion induces soliton instabilities, leading to the Cherenkov-type emission of dispersive waves [45,46] phase-matched with the soliton, as discussed in the extensive literature (see, e.g., [28,47]). This resonant dispersive-wave emission gives rise to a spectral band cen-

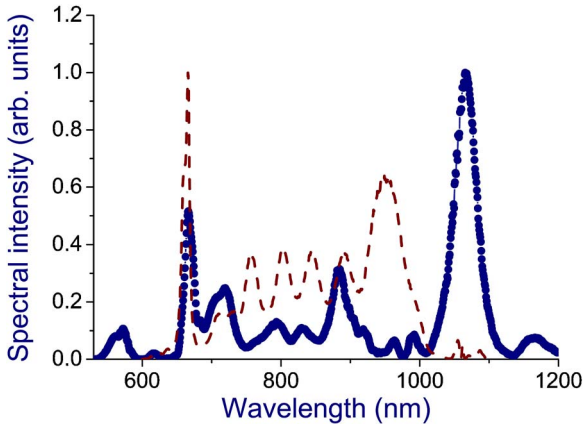

FIG. 6. (Color online) Filled circles connected with a solid line show experimental spectra measured at the output of a 20-cm NL-PM-750 fiber. The dashed line presents the input spectrum, provided by the Ti:sapphire oscillator.

tered around 540 nm in Fig. 5. As a result of the above-described nonlinear-optical transformations, the spectrum of the radiation field for a PCF with a characteristic length of 20 cm typically features four isolated bands, representing the remainder of the FWM-converted pump field (the bands centered at 670 and 900 nm in Fig. 5), the redshifted solitonic part (reaching 1.06 μm for $z=24$ cm in Fig. 5), and the blue-shifted band related to the Cherenkov emission of dispersive waves in the visible. In the time domain, as can be seen from Figs. 2(a) and 2(b), only the solitonic part of the radiation field remains well-localized in the form of a short light pulse, the remaining part of the field spreading out over a few picoseconds.

Our theoretical model, as can be seen from the comparison of the theoretical and experimental spectra of PCF output (Figs. 5 and 6), gives interesting physical insights into the soliton dynamics of few-cycle pulses in PCFs. Based on the results of simulations presented in Fig. 5, we identify the peaks at 550 and 1060 nm in Fig. 6 as the signatures of Cherenkov emission of dispersive waves and the redshifted soliton, respectively. The prominent peaks at 670 and 890 nm in Fig. 6 are indicative of phase-matched FWM processes around the zero-GVD wavelength, which give rise, as shown in Fig. 5, to two characteristic peaks at 650 nm and around 920 nm and deplete the pulse spectrum between these wavelengths. Energy conversion to the redshifted peak at 1.06 μm in Figs. 5 and 6 is indicative of a Raman-induced soliton self-frequency shift.

Replacement of chirped mirrors in the Ti:sapphire oscillator modifies the output spectrum of the laser, providing a higher spectral intensity within the range of wavelengths from 750 to 950 nm (line 4 in Fig. 1), but leaving the pulse width virtually unchanged. In Fig. 7, we present the simulated spectral evolution of such an input field in a PCF with a dispersion profile shown by curve 2 in Fig. 1. The spectrum of PCF output in this case again features signatures of self-phase modulation and four-wave mixing in the central part of the spectrum and well-resolved peaks corresponding to a redshifted soliton and Cherenkov emission of dispersive waves. However, with more energy of the input field concentrated in the near-infrared part of the spectrum, redshifted solitons with longer central wavelengths are generated at the output of PCF. The frequency-shifted soliton in the output spectrum of a 20-cm PCF in Fig. 7 is observed as an isolated peak centered at 1310 nm. This finding demonstrates the possibility of controlling the central wavelength of redshifted soli-

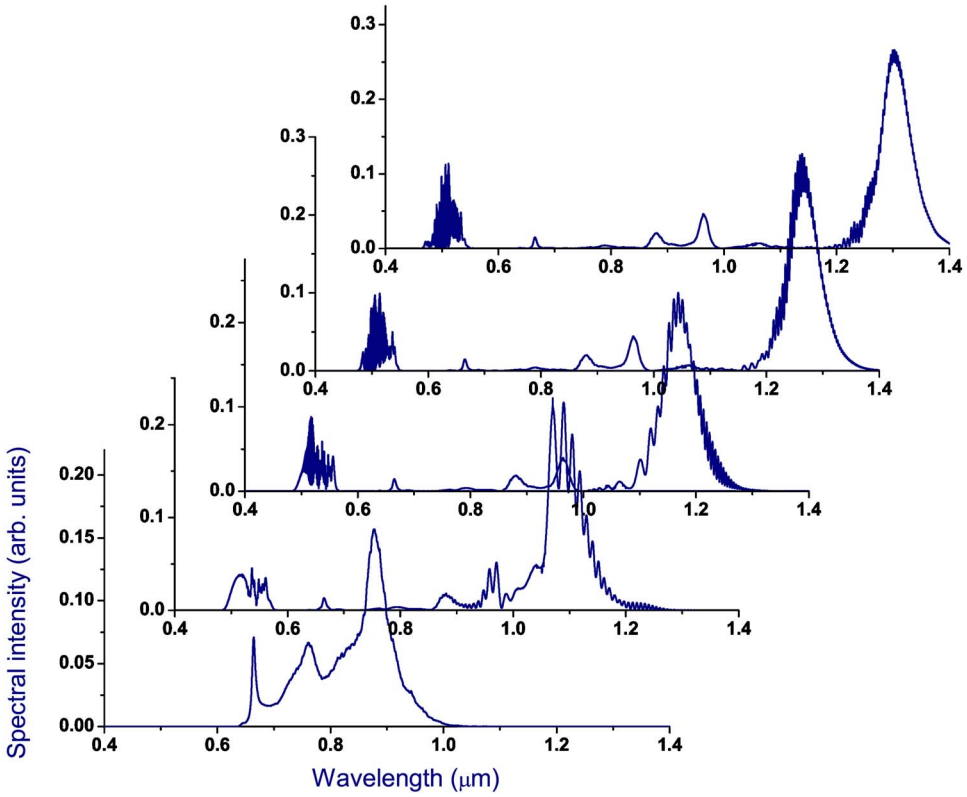

FIG. 7. (Color online) Spectral evolution of a laser pulse with an initial pulse width of 6 fs, an initial energy of 0.35 nJ, and an input spectrum shown by line 4 in Fig. 1 propagating through a PCF with a dispersion profile as presented by curve 2 in Fig. 1.

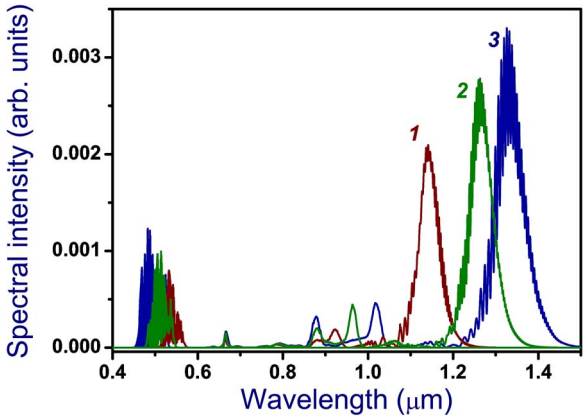

FIG. 8. (Color online) Spectra of radiation intensity at the output of a 20-cm PCF with a dispersion profile shown by curve 2 in Fig. 1 calculated for input pulses with an initial pulse width of 6 fs, intensity spectrum as presented by line 4 in Fig. 1, and an initial energy of 0.25 nJ (1), 0.35 nJ (2), and 0.45 nJ (3).

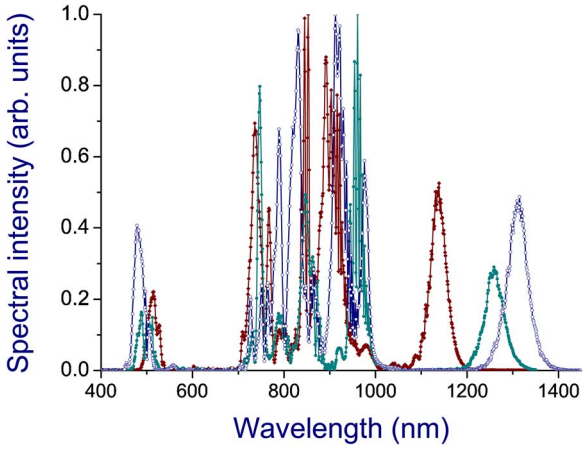

FIG. 9. (Color online) Experimental spectra at the output of a 20-cm NL-PM-750 fiber measured for three different input energies in the fundamental mode of the PCF, with the total energy of the 6-fs pulse coming to the objective equal to 2 nJ. The input spectrum of laser pulses is shown by line 4 in Fig. 1.

tons at the output of PCFs by modifying the spectrum of the input pulse.

Results of simulations presented in Fig. 8 illustrate the generation of wavelength-tunable redshifted soliton spectral component in a 20-cm PCF by input few-cycle pulses with a variable initial energy. As the energy of the input pulse increases from 0.25 to 0.45 nJ, the central wavelength of the redshifted soliton in Fig. 8 is tuned from 1.14 to 1.35 μm. The maximum wavelength shift of the soliton component with respect to the central wavelength of the laser pulse (defined as 800 nm for the Ti:sapphire oscillator) can thus reach 550 nm.

In experiments, the radiation energy launched into the fundamental mode of a 20-cm NL-PM-750 fiber was varied by translating and slightly tilting the in-coupling objective with respect to the input end of the fiber. The input radiation energy coupled into the fundamental mode of the fiber was used as a fitting parameter in our simulations and was defined from the best fit between the simulated spectra and the experimental data. In Fig. 9, we plot the normalized spectra measured at the output of a 20-cm NL-PM-750 fiber for three different input energies in the fundamental mode of the PCF, with the total energy of the 6-fs pulse coming to the objective being about 2 nJ. Our simulations provide a reasonable fit for the redshifted soliton parts of PCF output spectra, as well as for the blueshifted Cherenkov emission in the visible with the input energy in the fundamental mode ranging from 0.25 to 0.45 nJ (cf. Figs. 8 and 9). Discrepancies between results of simulations and experimental data, observed in the central part of the output PCF spectrum in Fig. 9, can be attributed to nonlinear-optical transformation of laser pulses guided in higher order modes of the PCF, as well as to cw radiation from the laser oscillator induced by backreflection from the fiber. Experimental results presented in Fig. 10 demonstrate a smooth tuning of the central wavelength of the redshifted PCF output of a PCF within the range 970 to 1170 nm by varying the input energy in the fundamental mode of the fiber. By adjusting the input energy coupled into the fundamental mode from 0.1 to 0.5 nJ, as can be seen from the experimental data shown in Figs. 9 and 10, we were able to generate a redshifted solitonic component at the output of the PCF with any wavelength from 970 nm (corresponding to the low-frequency edge of the input spectrum) to 1.35 μm.

To get an access to the evolution of laser pulses in the process of propagation along the fiber, we measured the spectra of radiation at the output of PCFs as a function of the fiber length. The length of the second-type PCF with a core diameter of 2.6 μm (inset 2 in Fig. 1) was gradually reduced in these experiments by the destructive cutback approach with input pulse parameters remaining unchanged (the input spectrum of the laser pulse is shown in the inset to Fig. 11). These measurements yielded a series of PCF output spectra, visualizing the spectral transformation dynamics of few-cycle pulses in the PCF. As shown in Fig. 11, the main spectral features of PCF output are adequately described by the GNSE. In particular, our theoretical model quite accurately predicts the central wavelengths and the amplitudes of the redshifted solitonic components, as well as their counterparts

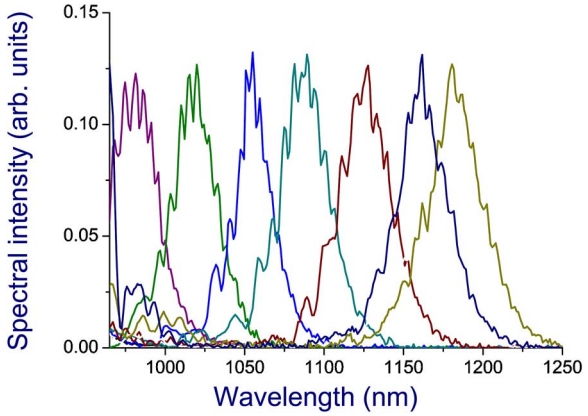

FIG. 10. (Color online) Experimentally measured redshifted output of the NL-PM-750 fiber tuned from 970 to 1170 nm by varying the input energy in the fundamental mode of the PCF.

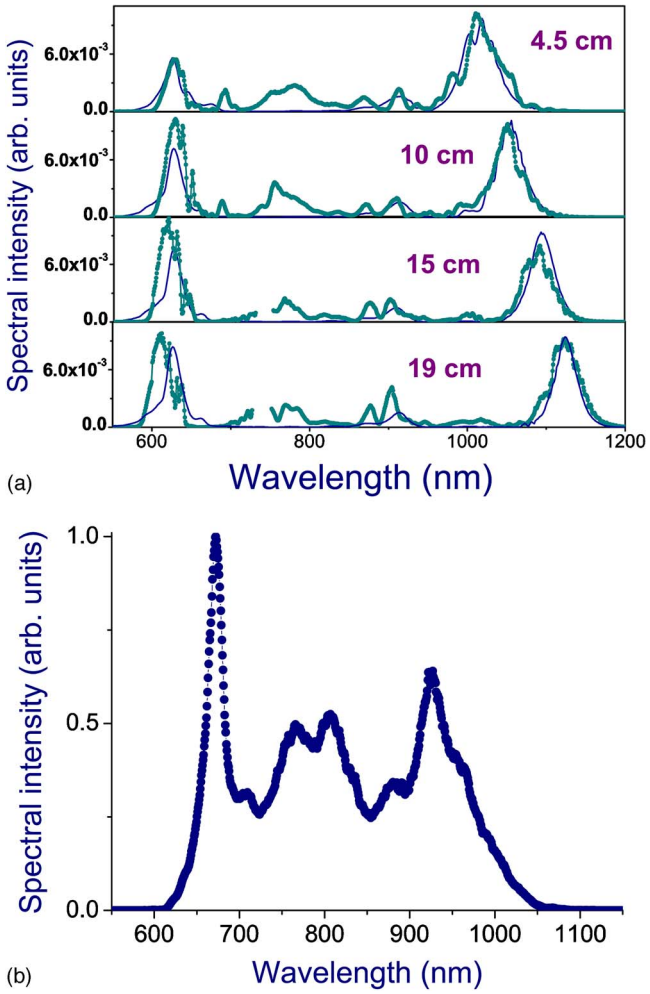

FIG. 11. (Color online) Output spectra measured (circles) and calculated (solid line) for a 2-nJ few-cycle laser pulse (the input spectrum is shown in the inset) transmitted through a silica PCF with a core diameter of 2.6 μm and a variable length—from top to bottom: 4.5, 10, 15, and 19 cm.

in the anti-Stokes part of the spectrum, originating from dispersive-wave emission. In the central part of the output spectrum, however, the experimental data can noticeably deviate from the results of GNSE simulations. While the model predicts a total depletion for the spectral components corresponding to the input field, experiments visualize a measurable part of output radiation energy within the range of wavelengths from 650 to 950 nm. Curve 2 in Fig. 12 displays the integral of the measured spectral intensity $S(\lambda)$, $F(\lambda)=\int_{\lambda_{\min}}^{\lambda} S(\lambda')d\lambda'$, where $\lambda_{\min}$ is the lower bound of the wavelength range covered by the detection system, as a function of the wavelength λ. As can be seen from this plot, the nonsolitonic part of output radiation, which includes the dispersive-wave component centered at 625 nm and the nondepleted central part of the spectrum, may contain up to 50% of the total radiation energy at the output of the fiber. This discrepancy between theoretical predictions and experimental results can be indicative of physical processes not included in the model, such as the excitation of higher order PCF modes and spatial self-action phenomena [48].

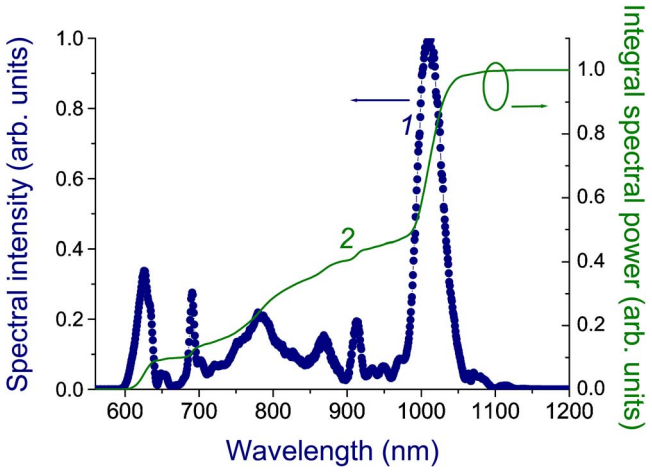

FIG. 12. (Color online) Output spectrum of a 3-cm PCF with a core diameter of 2.6 μm (1) and the corresponding integral of the spectral intensity $F(\lambda)$ as a function of the wavelength λ (2).

The key advantages of the SSFS-based strategy of widely tunable frequency shifting of few-cycle laser pulses demonstrated in this work originate from the intrinsic properties of Raman-shifted solitons. In particular, the central frequency of the redshifted soliton can be tuned by varying the fiber length and the input pulse energy. Radiation energy carried by this signal is localized in the time domain within a short spike, dominating the temporal envelope of radiation intensity in the fiber. Because of the anomalous group-velocity dispersion of the PCF, the redshifted soliton becomes delayed and eventually isolated, both spectrally and temporally, with respect to the rest of the pump field [Figs. 2(a) and 2(b)]. This isolation of the frequency-shifted soliton suppresses the interference between the solitonic part and the rest of the spectrum of radiation field. For a PCF with a characteristic length of tens of centimeters, the amplitude of the soliton spike in the temporal envelope of radiation intensity is typically an order of magnitude higher than the intensity of the remainder of SPM-broadened pump field and Cherenkov emission, both of which are spread out in time. As a result, the frequency-shifted solitonic component is observed in experiments as the most stable part of the output spectrum, which is free of intereference fringes, typical of the nonsolitonic part of the radiation field, including Cherenkov emission. Redshifted soliton signals formed by sub-6 -fs laser pulses in PCFs have been demonstrated to be ideally suited as a seed for optical parametric chirped-pulse amplification [37] and offer much promise as short-pulse light sources for spectroscopic and time-resolved pump–probe measurements.

V. CONCLUSION

We have shown in this work that photonic-crystal fibers can provide a highly efficient and widely tunable frequency shifting of few-cycle laser pulses through the soliton self-frequency shift induced by the Raman effect. With the wavelength of zero group-velocity dispersion of the fiber lying within the broad spectrum of the input pulse, the output spec-

tra observed in our experiments are dominated by distinct spectral peaks, originating from concurrent nonlinear-optical processes. We have identified well-resolved signatures of soliton self-frequency shift, four-wave mixing, and Cherenkov emission of dispersive waves and demonstrate that the laser pulse energy can be efficiently coupled into a spectrally isolated wavelength-tunable redshifted soliton peak. For this spectral peak, wavelength shifts as large as 500 nm have been demonstrated with input few-cycle Ti:sapphire laser pulses having broadband spectra centered at approximately 820 nm. The central wavelength of the redshifted output of a photonic-crystal fiber was smoothly tuned in our experiments from the low-frequency edge in the spectrum of the 6-fs Ti:sapphire laser pulse up to 1.35 μm by varying the input energy in the fundamental mode of the fiber.

ACKNOWLEDGMENTS

We are grateful to K.V. Dukel'skii, A.V. Khokhlov, Yu.N. Kondrat'ev, and V.S. Shevandin for fabricating fiber samples. E.E.S. and A.M.Z. acknowledge a partial support of their research by the Russian Foundation for Basic Research (Projects No. 06-02-16880-a, No. 04-02-39002-GFEN2004 and No. 05-02-90566-NNS), the Russian Federal Research and Technology Program (Contract No. 02.434.11.2010), and INTAS (Projects No. 03-51-5037 and No. 03-51-5288). This project was also supported in part by the LaserLab Europe and XTRA European networks. The research described in this publication was made possible in part by Grant No. RUP2-2695 of the U.S. Civilian Research & Development Foundation for the Independent States of the Former Soviet Union (CRDF).

[1] *Few-Cycle Laser Pulse Generation and Its Applications*, edited by F. X. Kärtner (Springer, Berlin, 2004).
[2] T. Brabec and F. Krausz, Rev. Mod. Phys. **72**, 545 (2000).
[3] *Ultrafast Phenomena XIV*, Proceedings of the 14th International Conference, Niigata, Japan, edited by T. Kobayashi, T. Okada, T. Kobayashi, K. A. Nelson, and S. De Silvestri (Springer, Berlin, 2005).
[4] T. Udem, R. Holzwarth, and T. W. Hänsch, Nature (London) **416**, 233 (2002).
[5] *Ultrafast Photonics*, edited by A. Miller, D. T. Reid, and D. M. Finlayson (Institute of Physics Publishing, Bristol, 2004).
[6] G. Cerullo, M. Nisoli, S. Stagira, and S. De Silvestri, Opt. Lett. **23**, 1283 (1998).
[7] A. Baltuška, T. Fuji, and T. Kobayashi, Phys. Rev. Lett. **88**, 133901 (2002).
[8] C. Manzoni, G. Cerullo, and S. De Silvestri, Opt. Lett. **29**, 2668 (2004).
[9] A. Dubietis, G. Jonušaskas, and A. Piskarskas, Opt. Commun. **88**, 437 (1992).
[10] R. Butkus, R. Danielius, R. Dubietis, A. Piskarskas, and A. Stabinis, Appl. Phys. B **79**, 693 (2004).
[11] C. P. Hauri, P. Schlup, G. Arisholm, J. Biegert, and U. Keller, Opt. Lett. **29**, 1369 (2004).
[12] R. T. Zinkstok, S. Witte, W. Hogervorst, and K. S. E. Eikema, Opt. Lett. **30**, 78 (2004).
[13] N. Ishii, L. Turi, V. S. Yakovlev, T. Fuji, F. Krausz, A. Baltuška, R. Butkus, G. Veitas, V. Smilgevicius, R. Danielius, and A. Piskarskas, Opt. Lett. **30**, 567 (2005).
[14] S. Witte, R. T. Zinkstok, W. Hogervorst, and K. S. E. Eikema, Opt. Express **13**, 4903 (2005).
[15] P. St. J. Russell, Science **299**, 358 (2003).
[16] J. C. Knight, Nature (London) **424**, 847 (2003).
[17] W. J. Wadsworth, A. Ortigosa-Blanch, J. C. Knight, T. A. Birks, T. P. M. Mann, and P. St. J. Russell, J. Opt. Soc. Am. B **19**, 2148 (2002).
[18] D. A. Akimov, E. E. Serebryannikov, A. M. Zheltikov, M. Schmitt, R. Maksimenka, W. Kiefer, K. V. Dukel'skii, V. S. Shevandin, and Yu. N. Kondrat'ev, Opt. Lett. **28**, 1948 (2003).
[19] W. H. Reeves, D. V. Skryabin, F. Biancalana, J. C. Knight, P. St. J. Russell, F. G. Omenetto, A. Efimov, and A. J. Taylor, Nature (London) **424**, 511 (2003).
[20] J. K. Ranka, R. S. Windeler, and A. J. Stentz, Opt. Lett. **25**, 25 (2000).
[21] *Supercontinuum Generation*, edited by A. M. Zheltikov, special issue of Appl. Phys. B **77**, 143 (2003).
[22] D. J. Jones, S. A. Diddams, J. K. Ranka, A. Stentz, R. S. Windeler, J. L. Hall, and S. T. Cundiff, Science **288**, 635 (2000).
[23] R. Holzwarth, T. Udem, T. W. Hänsch, J. C. Knight, W. J. Wadsworth, and P. St. J. Russell, Phys. Rev. Lett. **85**, 2264 (2000).
[24] I. Hartl, X. D. Li, C. Chudoba, R. K. Rhanta, T. H. Ko, J. G. Fujimoto, J. K. Ranka, and R. S. Windeler, Opt. Lett. **26**, 608 (2001).
[25] S. O. Konorov, D. A. Akimov, E. E. Serebryannikov, A. A. Ivanov, M. V. Alfimov, and A. M. Zheltikov, Phys. Rev. E **70**, 057601 (2004).
[26] H. N. Paulsen, K. M. Hilligsøe, J. Thøgersen, S. R. Keiding, and J. J. Larsen, Opt. Lett. **28**, 1123 (2003).
[27] S. O. Konorov and A. M. Zheltikov, Opt. Express **11**, 2440 (2003).
[28] D. V. Skryabin, F. Luan, J. C. Knight, and P. St. J. Russell, Science **301**, 1705 (2003).
[29] E. M. Dianov, A. Ya. Karasik, P. V. Mamyshev, A. M. Prokhorov, V. N. Serkin, M. F. Stel'makh, and A. A. Fomichev, JETP Lett. **41**, 294 (1985).
[30] F. M. Mitschke and L. F. Mollenauer, Opt. Lett. **11**, 659 (1986).
[31] G. P. Agrawal, *Nonlinear Fiber Optics* (Academic, San Diego, 2001).
[32] X. Liu, C. Xu, W. H. Knox, J. K. Chandalia, B. J. Eggleton, S. G. Kosinski, and R. S. Windeler, Opt. Lett. **26**, 358 (2001).
[33] B. R. Washburn, S. E. Ralph, P. A. Lacourt, J. M. Dudley, W. T. Rhodes, R. S. Windeler, and S. Coen, Electron. Lett. **37**, 1510 (2001).
[34] J. H. Price, K. Kurosawa, T. M. Monro, L. Lefort, and D. J. Richardson, J. Opt. Soc. Am. B **19**, 1286 (2002).
[35] K. S. Abedin and Fumito Kubota, Opt. Lett. **28**, 1760 (2003).

[36] E. E. Serebryannikov, A. M. Zheltikov, N. Ishii, C. Y. Teisset, S. Köhler, T. Fuji, T. Metzger, F. Krausz, and A. Baltuška, Phys. Rev. E **72**, 056603 (2005).
[37] C. Y. Teisset, N. Ishii, T. Fuji, T. Metzger, S. Köhler, R. Holzwarth, A. Baltuška, A. M. Zheltikov, and F. Krausz, Opt. Express **13**, 6550 (2005).
[38] X. Fang, N. Karasawa, R. Morita, R. S. Windeler, and M. Yamashita, IEEE Photonics Technol. Lett. **15**, 233 (2003).
[39] K. J. Blow and D. Wood, IEEE J. Quantum Electron. **25**, 2665 (1989).
[40] T. M. Monro, D. J. Richardson, N. G. R. Broderick, and P. J. Bennet, J. Lightwave Technol. **18**, 50 (2000).
[41] http://www.crystal-fibre.com/
[42] J. P. Gordon, Opt. Lett. **11**, 662 (1986).
[43] T. Brabec and F. Krausz, Phys. Rev. Lett. **78**, 3282 (1997).
[44] T. Fuji, A. Unterhuber, V. S. Yakovlev, G. Tempea, A. Stingl, F. Krausz, and W. Drexler, Appl. Phys. B **77**, 125 (2003).
[45] P. K. A. Wai, H. H. Chen, and Y. C. Lee, Phys. Rev. A **41**, 426 (1990).
[46] N. Akhmediev and M. Karlsson, Phys. Rev. A **51**, 2602 (1995).
[47] J. Herrmann, U. Griebner, N. Zhavornokov, A. Husakow, D. Nickel, J. C. Knight, W. J. Wadsworth, P. St. J. Russell, and G. Korn, Phys. Rev. Lett. **88**, 173901 (2002).
[48] A. L. Gaeta, Phys. Rev. Lett. **84**, 3582 (2000).